NUMERICAL INVESTIGATION ON THE VERTICAL WATER-ENTRY OF A HOLLOW CYLINDER AT LOW VELOCITY

Yu Hou, Zhen-Gui Huang, Zhi-Hua Chen, Ze-Qing Guo and Yu-Chuan Luo
National Key Laboratory of Transient Physics, Nanjing University of Science and Technology, Nanjing 210094, China

Based on the volume of fluid (VOF) multiphase flow equations, the *k-ε* turbulent model and sliding mesh technique, the low speed vertical water-entry of a hollow cylinder was investigated numerically. The numerical results have a good agreement with corresponding experimental results and finer mesh independence. The results show that a jet flow induced by the through-hole provides a new connection between the inner and outer flow at the pinch-off time underwater. Furthermore, a little bubble on the top of the through-hole jet is created by the collision of the edge surface of the water column inside the cylinder. The initial water-entry speed has a significant influence on the inner cavity formation, the pinch-off depth, the through-hole jet ejection and the motion parameter during the vertical water-entry process.

Keywords: Vertical water-entry, Hollow cylinder, Numerical simulation, Low water-entry speed, Multiphase flow

INTRODUCTION

The water entry problem of a solid object impacting on a liquid surface has challenged researchers for centuries, which is first studied systematically by Worthington [1] in the 19th century about the air-entraining cavity, splashes and closure jets of spheres coated with single-flash photography. Then Gilbarg and Anderson [2] discussed the effect of water-entry velocity and atmospheric pressure on the entraining cavity evolution of solid spheres. Richardson et al [3] studied the cavity formation and hydrodynamic resistance to spheres during the vertical water-entry. After that, May et al. [4, 5] considered extensive factors on the cavity formation with including the entry speed, atmospheric pressure and sphere radius. The resistance coefficients of rigid spheres with different radiuses and entry speeds were studied systematically. Duez et al. [6], Aristoff and Bush [7] investigated the influence of

hydrophilic and hydrophobic surface of spheres on the cavity formation respectively by conducting controlled experiments.

The structure and material of entry model are studied more extensively on recent researches to meet the practical needs. Chen [8] studied entry cavity flow characteristics of projectiles with three warhead shapes at different entry speed. He [9] carried out water entry experiments on the cylinder with various initial velocity and attitudes. Truscott et al. [10] reviewed the experimental researches on spheres and slender bodies with cone, cusp, ogive and flat heads. Lu et al. [11] studied the vertical water entry of a semi-closed cylinder experimentally, which illustrated the hydrodynamic characteristics of fluctuation cavitation pattern when the water poured to the cylindrical shell.

The theoretical work of water entry problem is carried out by von Karman [12] and Wagner [13], who investigated the phenomenon related to the impact of objects on liquid surfaces. They considered the solid body entering a fluid at large Reynolds and Weber numbers, where viscosity and surface tension were neglected. In the recent years, there has been a growing interest in the physics of impact, particularly due to the development of computer. Greenhow [14] simulated the free surface deformations of initially calm water caused by the impact of a horizontal circular cylinder by using a nonlinear two-dimensional numerical calculation. Lin [15] developed a two-dimensional numerical model to simulate a moving body in a free surface flow based on the cut-cell technique in a fixed-grid system, and the volume of fluid (VOF) method was applied to track interface.

Compared to solid objects on the above researches, few studies on the water entry problem of hollow structures are carried out. According to the published work, Tseitlin [16] first proposed that the solution of the plane problem of flow past two flat plates be extended to flow past the disc with a hole. Deinekin [17] numerically solved the problem of axisymmetric flow past a ducting cavitator. Savchenko [18] studied the resistance characteristics of disc cavitation with different apertures through water tunnel experiments. The free-surface impact of hollow structure results in complex flow fields both inside and outside, which has more study challenges involved in multiphase flow than hollow projectiles [19] in the air. Meanwhile, several parameters of the through-hole in the structure such as size, quantity, pattern and opening position will affect the navigation resistance, the stealth and the trajectory stability of the vehicle underwater.

Therefore, the investigation on the water-entry of hollow structures is of great significance for the design and improvement of airdrop torpedoes and sonar buoys, drainage holes and discharge orifices of a submarine, etc. In this paper, the water entry of a hollow cylinder is investigated by numerical simulation. The numerical and experimental results are compared to validate the numerical method. Then several cases of the water entry with the increasing entry speed are illustrated. The trajectories, velocities, accelerations of the cylinder and the drag coefficient during water entry are also investigated.

NUMERICAL MODEL

Governing equations

The VOF model in the form of Reynolds-averaged Navier-Stokes equations is applied to describing the vertical water-entry cavities. The continuity equation for the mixture flow is

$$\frac{\partial \rho_m}{\partial t}+\frac{\partial(\rho_m u_j)}{\partial x_j}=0 \tag{1}$$

Where ρ_m=(1-α_{water}) ρ_{air}+α_{water} ρ_{water} represents the mixture density. ρ_{air} and ρ_{water} represent the air density and water density respectively. The water volume fraction α_{water}= 0.5 at the boundary between the air and water.

The momentum equations for the mixture flow is

$$\frac{\partial \rho_m u_i}{\partial t}+\frac{\partial(\rho_m u_i u_j)}{\partial x_j}=\rho_m g_i-\frac{\partial P}{\partial x_i}+\frac{\partial}{\partial x_j}[(\mu_m+\mu_t)(\frac{\partial u_i}{\partial x_j}+\frac{\partial u_j}{\partial x_i})] \tag{2}$$

where g_i represents the gravity acceleration in x_i coordinate. P represents the mixture pressure. μ_m=(1-α_{water}) μ_{air} +α_{water} μ_{water} represents the mixture dynamic viscosity coefficient and μ_t is the turbulent viscosity.

The two equation realizable k-ε turbulence model is used to set the viscous equation closed. The turbulent kinetic transport equation is

$$\frac{\partial(\rho_m k)}{\partial t}+\frac{\partial(\rho_m k u_i)}{\partial x_i}=\frac{\partial}{\partial x_i}[(\mu+\frac{\mu_t}{\sigma_k})\frac{\partial k}{\partial x_i}]+G_k+G_b-\rho_m\varepsilon-Y_M+S_k \tag{3}$$

The transport equation of dissipation rate of energy from the turbulent flow is

$$\frac{\partial(\rho_m \varepsilon)}{\partial t}+\frac{\partial(\rho_m \varepsilon u_i)}{\partial x_i}=\frac{\partial}{\partial x_i}[(\mu+\frac{\mu_t}{\sigma_\varepsilon})\frac{\partial \varepsilon}{\partial x_i}]+\rho C_1 S\varepsilon-\rho C_2\frac{\varepsilon^2}{k+\sqrt{\nu\varepsilon}}+C_{1\varepsilon}\frac{\varepsilon}{k}C_{3\varepsilon}G_b+S_\varepsilon \tag{4}$$

Where $C_1=\max[0.43,\frac{\eta}{\eta+5}]$, $\eta=S\frac{k}{\varepsilon}$, $S=\sqrt{2S_{ij}S_{ij}}$.

In these equations, G_k and G_b represent the generation of turbulence kinetic energy due to the mean velocity gradients and buoyancy respectively. Y_M represents the contribution of the fluctuating dilatation in the compressible turbulence to the overall dissipation rate. C_2 and $C_{1\varepsilon}$ are constants. σ_k and σ_ε are the turbulent prandtl numbers for k and ε, respectively. S_k and S_ε are source terms.

Model schematic and computational domain

The hollow projectile is simplified to a tubular cylinder in Fig.1 and specific dimension is shown in Table 1. As shown in Fig.2, an axisymmetric two-dimensional plane(15D×45D) was designed for the computational domain. The water depth is 30D and the test model falls freely at the height of 1.25D from the water surface in gravity. The operating pressure P_0 is 101325Pa. The stationary wall was chosen for both side and bottom boundary. The top boundary is pressure-inlet. The impact time and the water-entry location are defined as the origin of time and x coordinate respectively.

In the present paper, the structured mesh is employed throughout the whole domain for the mesh generation using the commercial software ANSYS ICEM, as shown in Fig.3. The grid dimension increases gradually from the cylinder boundary to the domain boundary. The mesh contains 906322 elements and the minimum mesh size is 2.14×10^{-4}m.

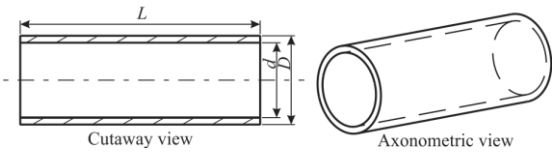

Figure 1. Schematic of the hollow cylinder.

TABLE 1. DETAILS OF THE HOLLOW CYLINDER.

D **(mm)**	***d*** **(mm)**	***d/D***	***L*** **(mm)**	***M*** **(kg)**
30.0	25.3	0.84	80.0	0.128

Numerical Treatment

The numerical simulations were carried out by using ANSYS FLUENT software to solve Reynolds-Averaged Navier-Stokes (RANS) equations. The above time-dependent governing equations are discretized by using the finite volume method, and the SIMPLE scheme is used to solving the pressure-velocity coupling algorithms. The second order upwind scheme is used for the convection terms and the central-difference for the diffusion term in the momentum equations. The PRESTO (pressure staggering option) scheme is used for the pressure interpolation. The Geo-Reconstruct scheme is used for the transport equation for the volume fractions. The Realizable k-ε model with standard wall functions is carried out in the software FLUENT.

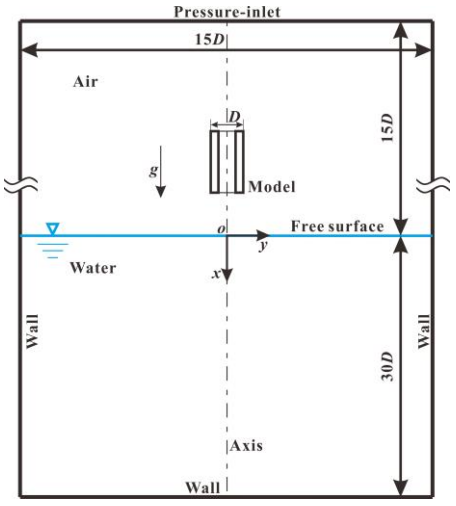

Figure 2. The computational domain and boundary conditions.

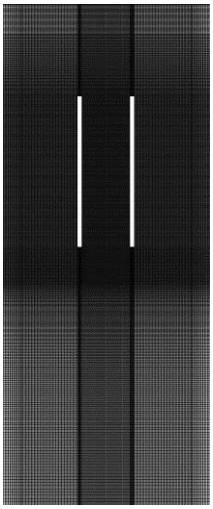

Figure 3. Mesh structure.

RESULTS AND DISCUSSION

Numerical Validation

The simulation results are compared directly with corresponding experimental results to validate the numerical methodology and meanwhile establish the grid independence in the present paper in Fig.4. The experimental result in Fig.4(a) and simulation results with increasing resolutions in Fig.4(b)~(g) at 25ms with the initial water-entry speed v_0=2.84m/s are present together. As illustrated in this case, a subsurface air cavity surrounds the hollow cylinder and a jet with a top bubble ejects through the hole after water entry. The numerical results agree well with the experiment results on the jets structure and splash shapes.

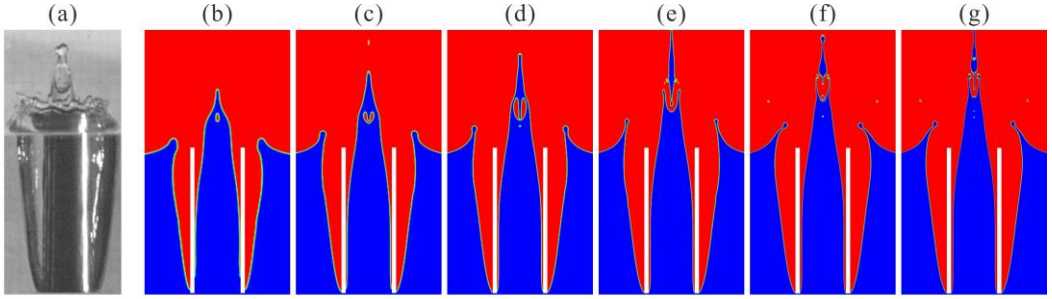

	(b)	(c)	(d)	(e)	(f)	(g)
Mesh quantity ($\times 10^4$):	46	68	90	120	200	270
Minimum mesh size($\times 10^{-4}$m):	3.92	2.94	2.14	1.96	1.24	0.90

Figure 4. Comparison of cavity formation and splash of experiment and simulation with different resolutions at 25ms.

In order to establish the grid independence, the number of the computational mesh elements increases from 0.46 million to 2.7 million and the grid size of the boundary layer is refined from 3.92×10^{-4}m to 0.90×10^{-4}m, as shown in Fig.4(b)~(g). The air cavity and splash have a clearer shape with the increasing numerical

resolution. The little bubble on the top of the through-hole jet is captured clearly in the simulation with mesh elements more than 0.9 million. No essential changes in the water-entry process are found with the further refinement except the discontinuous boundary of the top bubble within the margin of error. The volume and stretch shape of the through-hole jet and bubble remain the same approximately.

Moreover, the experimental and the numerical depth of the hollow cylinder with the increasing mesh quantity is shown in Fig.5. The results show that the numerical motion of the hollow cylinder has the same trend as the experiment. The depth error is reduced with the further refinement but the enormous computational cost must be solved. After comparing the cavity shape and the hollow cylinder depth, the finer mesh with 906322 elements is found to be applicable to improve simulated efficiency in the present paper.

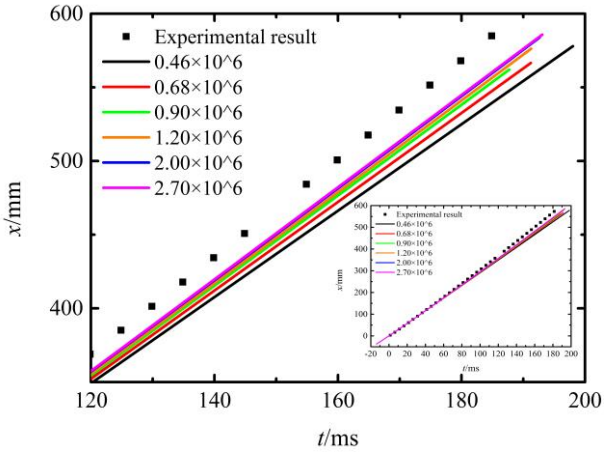

Figure 5. Comparison of the experimental and the numerical depth of the hollow cylinder with the increasing mesh quantity.

The entry cavity evolution with the increasing entry velocity

To investigate the air entraining cavity of the hollow cylinder with low vertical entry speed, the water-entry process was simulated. The entry speed v_0 is increased from 0.90m/s to 2.84m/s. Three typical cases of the vertical water-entry cavity evolution with entry speed v_0=0.90, 1.90, 2.84m/s are shown in Fig.6(a)~(c) respectively. The origin time (t=0ms) of the image record is defined as the impact moment. Four distinct stages are considered following the discussions of May [5] and Truscott et al. [10] the impact stage, the open cavity and jets growth stage, the pinch-off stage and the sailing stage with cavity attached.

When the hollow cylinder impacts the water surface, the autogenic succession of energy transfer makes the flow around the cylinder head obtain oblique inward and upward velocity, therefore, a jet inside the hole and a surrounding air cavity forms in the open cavity and jets growth stage respectively. The pierced flow moves backward to be the through-hole jet that has a regular geometric shape and an attached spherical bubble at the top. The surrounding flow expand outward to be an

axisymmetric air entraining cavity that wraps the cylinder. The pinch-off stage comes after the expansion end and the shrink beginning of the cavity wall with the potential energy of the fluid nearby transformed into the kinetic energy.

Then the cavity wall pinches off at a point on the through-hole jet or the bottom of the cylinder due to different entry velocities. Compared with the traditional deep closure at a point [5,9] under the free surface, the extrusive jet column inside the hole provides a further connection of the pierced flow and the surrounding flow and creates an annular bubble covering the through-hole column occurs when the closed cavity is cut off at the bottom of the cylinder. Finally, in the sailing stage with cavity attached, semi-closed surrounding cavity and two lathy "tails" of the shedding bubbles are found in the side view after the annular bubble was stretched.

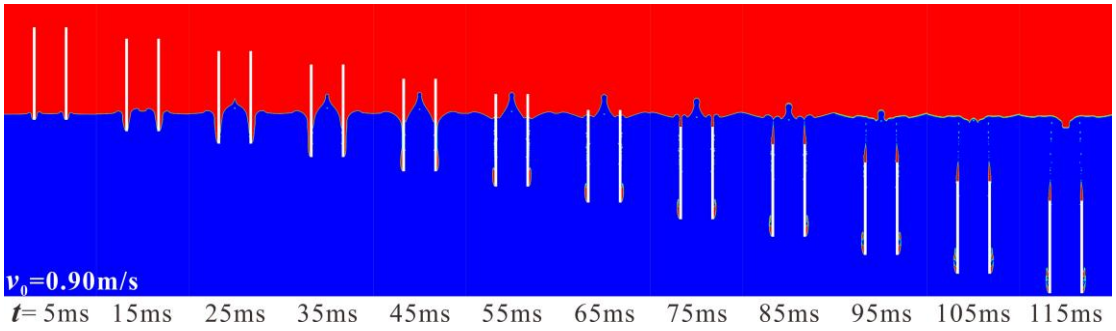

(a) Cavity evolution at the entry speed v_0=0.90m/s

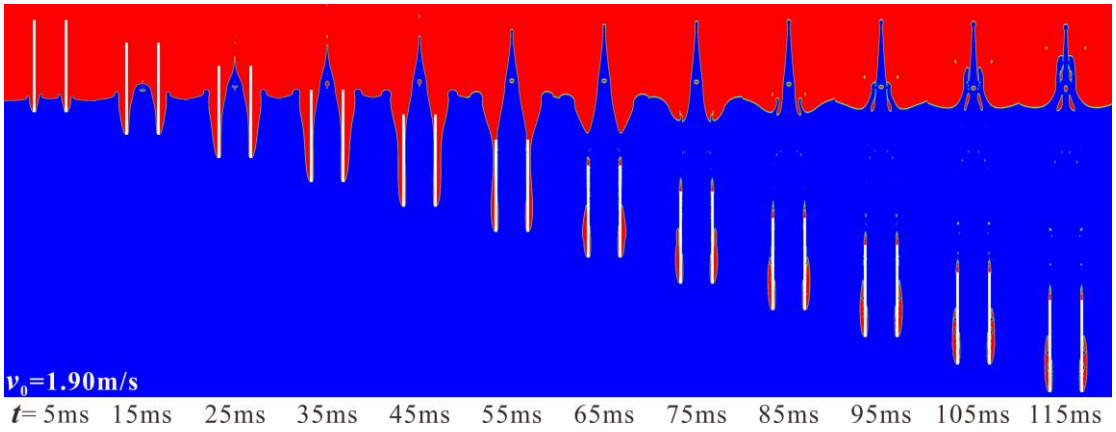

(b) Cavity evolution at the entry speed v_0=1.90m/s

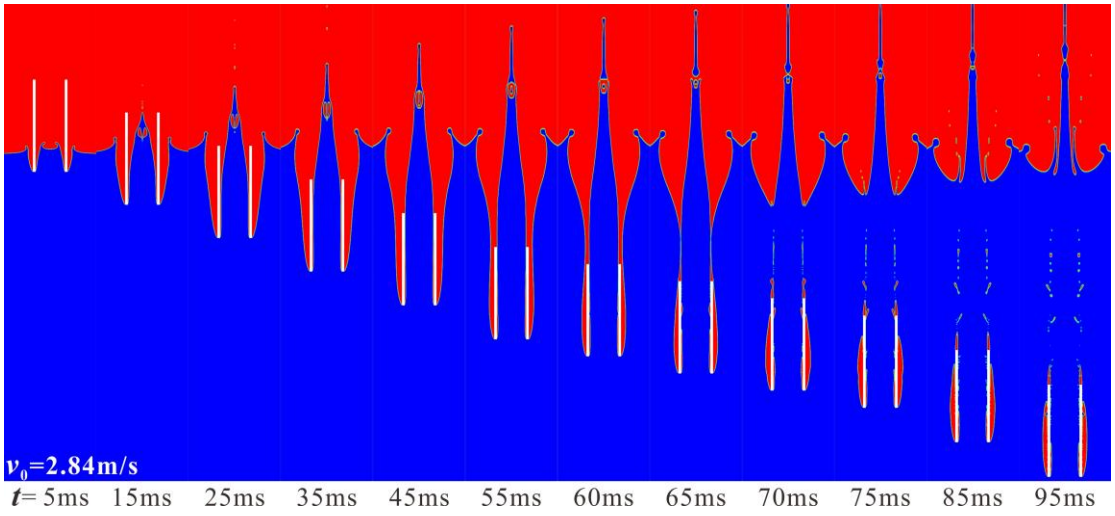

(c) Cavity evolution at the entry speed v_0=2.84.m/s

Figure 6. Three typical cases of the vertical water-entry cavity of the hollow cylinder with the increasing entry speed.

However, some specific flow changes are found with the increasing entry speed. First, there is no internal cavity on the through-hole wall when the entry speed is 0.90m/s, as shown in Fig.6(a) and Fig.7(a). The internal cavity forms and the volume of the cavity increases gradually when the entry speed grows larger than 1.30m/s, which is testified by changes of the dimensionless length lc/D shown in Fig.8(c) with the increasing entry speed. The length lc of the internal cavity at the first pinch-off time is defined in the partial enlargement(Fig.7(g)).

Moreover, the depth l of the pinch-off point defined in Fig.7(c)(f) and the maximum size dc of the air cavity defined in Fig.7(d) at the pinch-off time are in a positive correlation significantly with water entry speeds shown in Fig.8(a)(b). The pinch-off point moves upward from the first half of the outer wall to the bottom of it gradually with the increasing entry speed in Fig.7(a)~(f). The more kinetic energy transfer from the impact cylinder with higher entry speeds results in the more larger expansion of the air cavity wall and the postpone of the pinch-off. Furthermore, the increase of the ejection velocity of through-hole jets and the volume of top bubbles at the pinch-off time is observed with the rise of entry speeds in the Fig.7.

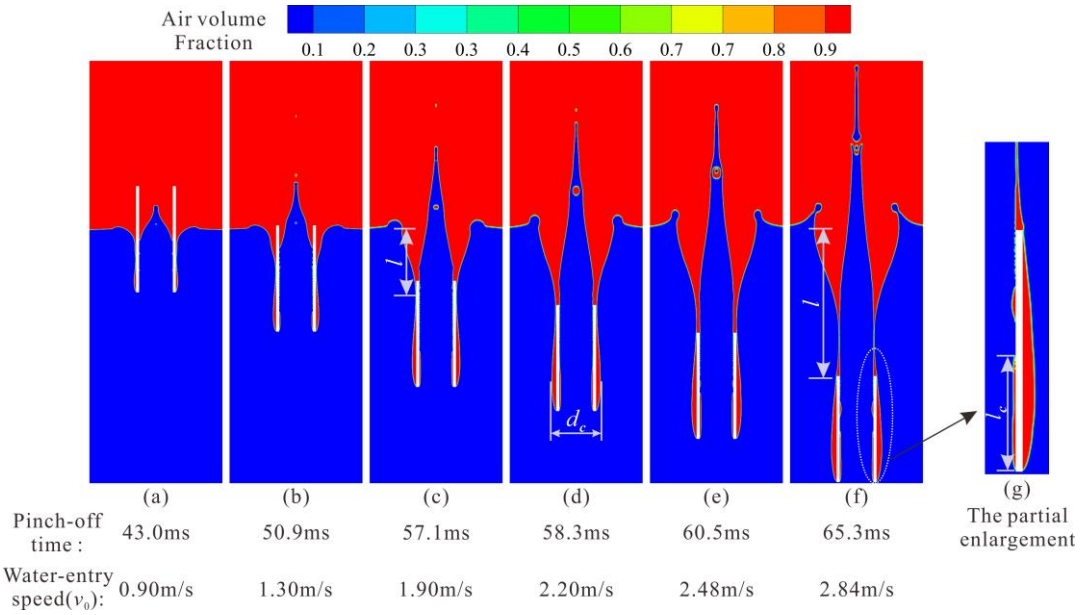

Figure 7. Comparison of the attached cavity in numerical and experimental results.

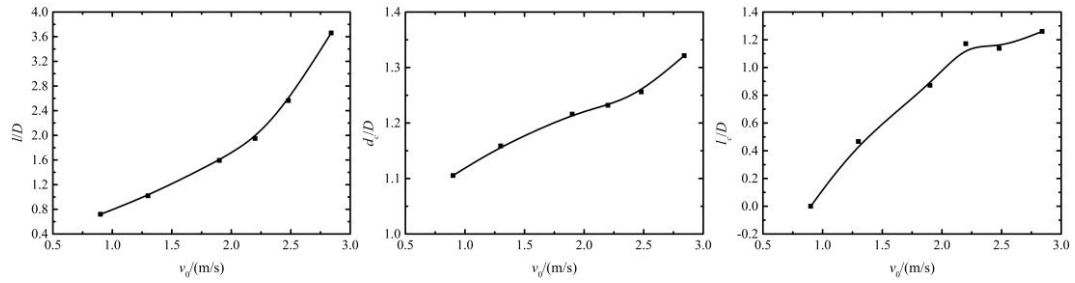

(a) (b) (c)

Figure 8. (a)The non-dimensional depth of closure points, (b)the maximum diameter of cavities and (c)the length of internal cavities at the first pinch-off time with the increasing entry speed.

In conclusion, the through-hole jets with top bubbles induced by the hollow structure during the water-entry process establish a new form of cavity wall shrinking change the seal mode of cavity wall comparing the traditional deep closure. The annular bubble following little shedding bubbles forms on the bottom of the moving body. Meanwhile, the entry speed has an obvious influence on the inner cavity formation, the pinch-off depth and the through-hole jet ejection.

Motion characteristics of the hollow cylinder with the increasing velocity

Main parameters of the hollow cylinder motion are shown in Fig.9(a)~(d), which include the transient displacement x, velocity v, acceleration a and dimensionless parameter v/v_0. The transient displacement x, velocity v and acceleration a are obtained from the numerical results. The drag coefficient $C_d=F/(0.5\rho v^2 A)$ changes with the increasing entry speed are present in Fig.10, where the total resistance is calculated by $F=-Ma+Mg$.

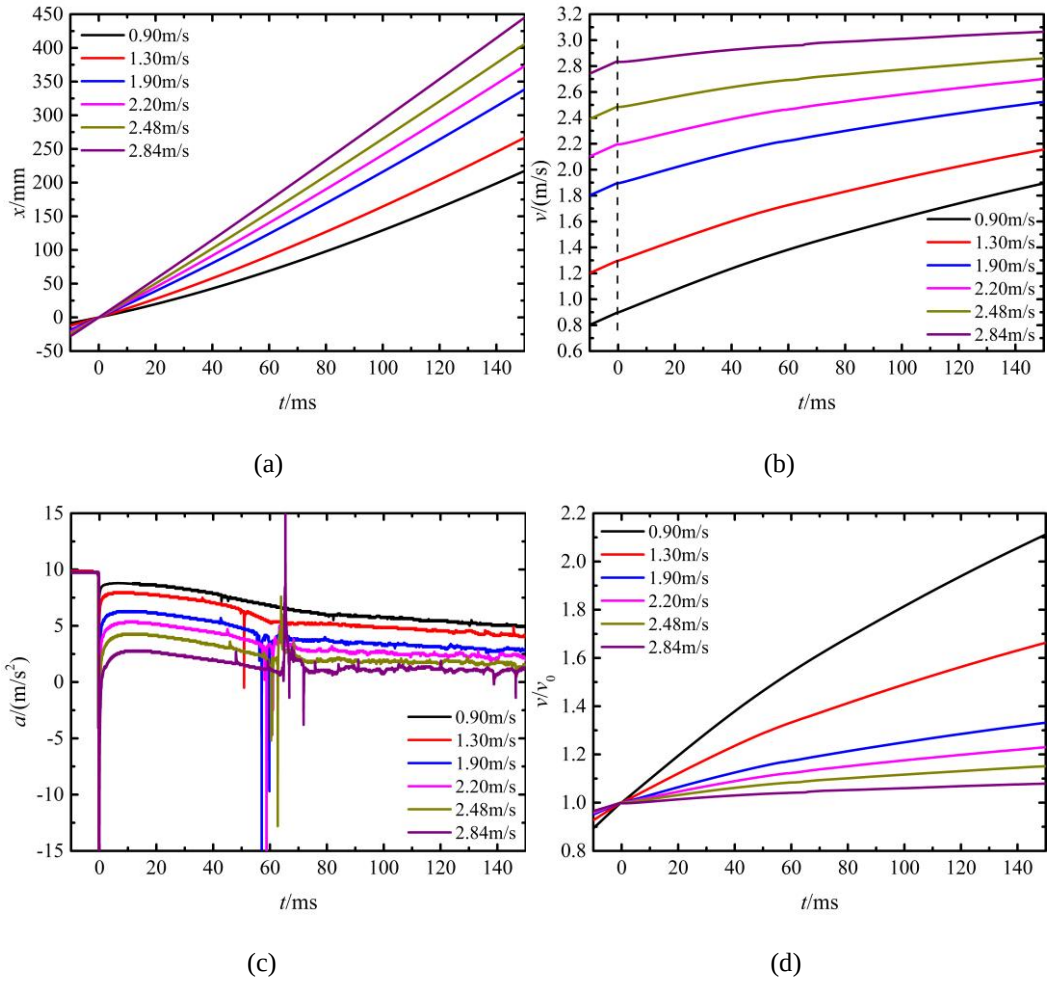

Figure 9. (a) The displacement, (b) the numerical velocity, (c) the numerical acceleration and (d) the dimensionless velocity of the hollow cylinder during the water-entry process with the increasing entry speed.

The motion of the hollow cylinder is divided into three stages including the free fall stage before the water-entry, the open cavity stage during the water-entry and the sailing stage with cavity attached after the deep-closure. The demarcation between these three stages are shown in Fig.9(c) and Fig.10 at the water-entry time (t=0ms) and the pinch-off time (t=40~70ms) clearly. The value of a remain gravitational acceleration 9.8m/s before the water entry and has a sharp decrease at the impact time. However, it recovers to be positive a moment later less than gravitational acceleration(g) and the difference grows with the increasing entry speed. The second demarcation comes with the surrounding pressure fluctuation due to the pinch-off at t=40~70ms. The acceleration has more significant fluctuations with the increasing water-entry speed, which is evidenced by the drag coefficient C_d in Fig.10 on the other hand. Meanwhile, The more significant acceleration fluctuations with the increasing entry speed results in the more obvious velocity growth shown in Fig.9(d).

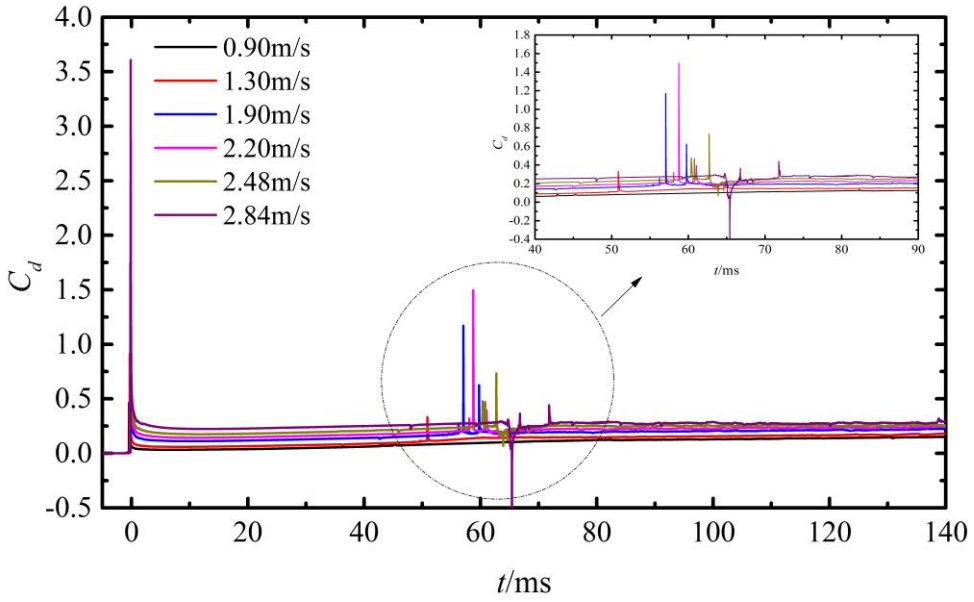

Figure 10. The numerical drag coefficient of the hollow cylinder with the increasing entry speed.

CONCLUSION

Numerical investigations on the low speed vertical water-entry of hollow cylinders with the increasing entry speeds were carried out. The simulation has good agreements in comparison with corresponding experimental data and finer mesh independence. Some insights into the flow characteristics during the water entry were predicted in consideration of the solid cylinder in reality. For the vertical water-entry hollow cylinders, a through-hole slender jet with a top bubble included near its head is created due to the collision of the edge surface of the water column. And it establishes a new form of cavity wall shrinking changing the deep closure pattern from a point closure to a horizontal circular arc closure underwater comparing the traditional deep closure. An annular bubble following little shedding bubbles forms on the bottom of the moving body. Meanwhile, the entry speed has an obvious influence on the inner cavity formation, the pinch-off depth and the through-hole jet ejection. The motion parameter modifications of the vertical water-entry hollow cylinder are divided into three stages by the entry point and the closure point, the free fall stage before the water-entry, the open cavity stage during the water-entry and the sailing stage with cavity attached.

ACKNOWLEDGMENTS

This work is supported by "the Key Laboratory Fund" No.61426040303162604004 and No.614260403041803, "the Fundamental Research Funds for the Central Universities" No.30917012101 and "the Postgraduate Research & Practice Innovation Program of Jiangsu Province" No.KYCX19_0259.

REFERENCES:

1. Worthington A M. 1882. "On Impact with a Liquid Surface" *Proceedings of the Royal Society of London*, 34(220): 217-230.
2. Gilbarg D, Anderson R A. 1948. "Influence of atmospheric pressure on the phenomena accompanying the entry of spheres into water" *Journal of Applied Physics*, 19(2): 127-139.
3. Richardson E G. 1948. "The impact of a solid on a liquid surface" *Proceedings of the Physical Society*, 61(4): 352.
4. May A, Woodhull J C. 1950. "The virtual mass of a sphere entering water vertically" *Journal of Applied Physics*, 21(12): 1285-1289.
5. May A. 1952. "Vertical entry of missiles into water" *Journal of Applied Physics*, 23(12): 1362-1372.
6. Duez C, Ybert C, Clanet C, Bocquet L. 2007. "Making a splash with water repellency" *Nature physics*, 3(3): 180-183.
7. Aristoff J M, Bush J W M. 2009. "Water entry of small hydrophobic spheres" *Journal of Fluid Mechanics*, (619): 45-78.
8. Chen X. 1985. "Experimental studies on the cavitation phenomena as a pellet entering water" *Explosion and Shock Waves*, 5(04): 70-73.
9. He C T. 2012. "Low speed water-entry of cylindrical projectile" *Acta Physica Sinica*, 61(13): 134701.
10. Truscott T T, Epps B P, Belden J. 2014. "Water Entry of Projectiles" *Annual Review of Fluid Mechanics*, 46(1): 355-378.
11. Lu Z L, Wei Y J, Cong W, Zhao S, Astronautics S O. 2016. "An experimental study of water-entry cavitating flows of an end-closed cylindrical shell based on the high-speed imaging technology" *Acta Physica Sinica*, 65(1): 14704.
12. Von Karman T. 1929. "The impact on seaplane floats during landing". *NACA Technical Report* 321.
13. Wagner H. 1932. "Phenomena associated with impacts and sliding on liquid surfaces" *Z. Angew. Math. Mech*, 12(4): 193-215.
14. Greenhow M. 1988. "Water-entry and-exit of a horizontal circular cylinder" *Applied Ocean Research*, 10(4): 191-198.
15. Lin P. 2007. "A fixed-grid model for simulation of a moving body in free surface flows" *Computers & fluids*, 36(3): 549-561.
16. Tseitlin M. 1959. "On the pressure on two parallel plates in a jet flow" *TsAGI Transactions on Hydrodynamics*, 01(01): 296-308.
17. Deinekin P. 1994. "Cavity flow past flow passage bodies" *Gidromekhanika*, 01(68): 74-78.
18. Savchenko G Y. 2012. "Hydrodynamic Characteristics of a Disc with Central Duct in a Supercavitation Flow". Berlin: Springer Berlin Heidelberg, pp. 107-113.
19. Sahu J, Heavey K R. 1996. "Chapter 41 - High performance parallel computing CFD simulations of projectiles with flow control". Parallel Computational Fluid Dynamics 2004, Winter G, Ecer AandFox P, et al, Amsterdam: Elsevier Science, 329-337.